TECHNICAL REVIEW

No.16 / September 2021

Technical Review

MAPNA TURBINE ENGINEERING & MANUFACTURING CO. (TUGA)

TUGA

MAPNA GROUP

Willpower to Empower Generations

Technical Review
MAPNA TURBINE ENGINEERING & MANUFACTURING CO. (TUGA)

Editorial & Production

Editorial Director:
Owliya, Mohammad

Production Director:
Jabery, Roohollah

Associate Editors:
Rashidi, Saeid
Sarmast, Mohammad

Graphic Designer:
Radfar, Kianoosh

Coordinator:
Azizi, Fakhrodin

Cover Page:
Additive Manufacturing on the Rise at MAPNA Turbine

Editorial

Dear Colleagues, Partners and Professionals,

MAPNA Group is dedicated to excellence and we try to take every conceivable opportunity for growth and perfection on our ambitious path towards greatness. That is why we are constantly busy reviewing and improving our products and manufacturing processes as well as the way we take care of our customers, whilst remaining as efficient and resilient as possible. It is in this context and with great pleasure that a brief account of a few recent achievements is presented to you, our valuable readers, in this edition of MAPNA Turbine Technical Review.

A case study performed on a fault occurred within the HRSG of a combined cycle power plant and its subsequent impact on the steam turbine performance is presented in the first article. The aim is to evaluate the performance of an Artificial-Intelligence-(AI) based Intelligent Condition Monitoring System (ICMS) developed by MAPNA Electric & Control Company (MECO) under actual working conditions. The predictions of the model seems to be perfectly congruent with the incidents on the ground, including repair and maintenance activities carried out to resolve the issue and restoring the performance of the equipment involved. This bodes well for further and future applications of the model.

The second article outlines meticulous steps taken to go through the entire additive manufacturing process of the fixing pieces of MGT-30 gas turbine combustion chamber as the first components to be put into action on the machine. Selection of the metal powder and specification of various parameters involved in the manufacturing and heat treatment process of the part providing best possible outcomes are also elaborated on.

A new specialized, pulse-echo ultrasonic test method developed to make possible in-situ inspection and assessment of MGT-70 gas turbine compressor vane tenons is featured in the third article. The developed method is capable of minute material loss detections of 0.5 mm deep and will bring about broader applications in the future by providing more versatile low cost inspection and maintenance services.

The fourth article is a profound story of a successful design and development of an in-house, tailor-made scoop sampling device following some careful analyses and experimental investigations. The sampler would make in-situ specimen extraction of critical power plant parts and equipment possible in a quite semi-destructive fashion for further analyses of in-service components from mechanical and micro-structural analyses to remnant life assessment.

Finally, the fifth article introduces MAPNA MIND platform developed within MAPNA Group (by MECO) to lead the way to the fourth industrial revolution by embracing digitalization and IIoT solutions. This will literally revolutionize the way the operational data is collected, synthetized and utilized to optimize multiple aspects in the operation and maintenance of turbines and plants.

Please join us in relishing the detailed account of these subjects, in this issue of the Technical Review.

Respectfully,

Mohammad Owliya, PhD

General Director
MAPNA Turbine Company (TUGA)
September 2021

Contents

1

Thermal Power Plant Condition Monitoring Using Artificial Intelligence & Thermodynamic Performance Indicators: A Case Study

Ghahremani, Arash
Yari, Mostafa
Rahimi Kelarijani, Mehrab
Aleahmad, Arash

MAPNA Electric & Control, Engineering & Manufacturing Co. (MECO)

Introduction

System performance condition monitoring has exhibited its significance more profoundly in recent years. The necessity for reducing costs and environmental impacts, as well as competitive markets in the energy sector have encouraged the industry practitioners to increase/maintain the efficiency of their assets as high as possible. Immediate fault diagnosis is one of the main elements of any attempt to enhance system's performance level which has attracted the attention of energy researchers.

In the current research, using an artificial intelligence model and thermodynamic key performance indicators (KPI), a case study of a fault in heat recovery steam generator (HRSG) has been investigated, and the effect of performance degradation has been determined on the steam turbine.

Case Study Power Plant

The studied power plant is of the combined cycle type comprising two gas turbines and HRSGs providing the steam required for the operation of a steam turbine set. The steam turbine is of single casing type with two HP and LP sections. The HRSG provides steam at two pressure levels of HP and LP feeding the HP and LP steam turbine sections, respectively. Fig. 1 represents configuration of the equipment and assets belonging to an individual combined cycle unit of the studied power plant.

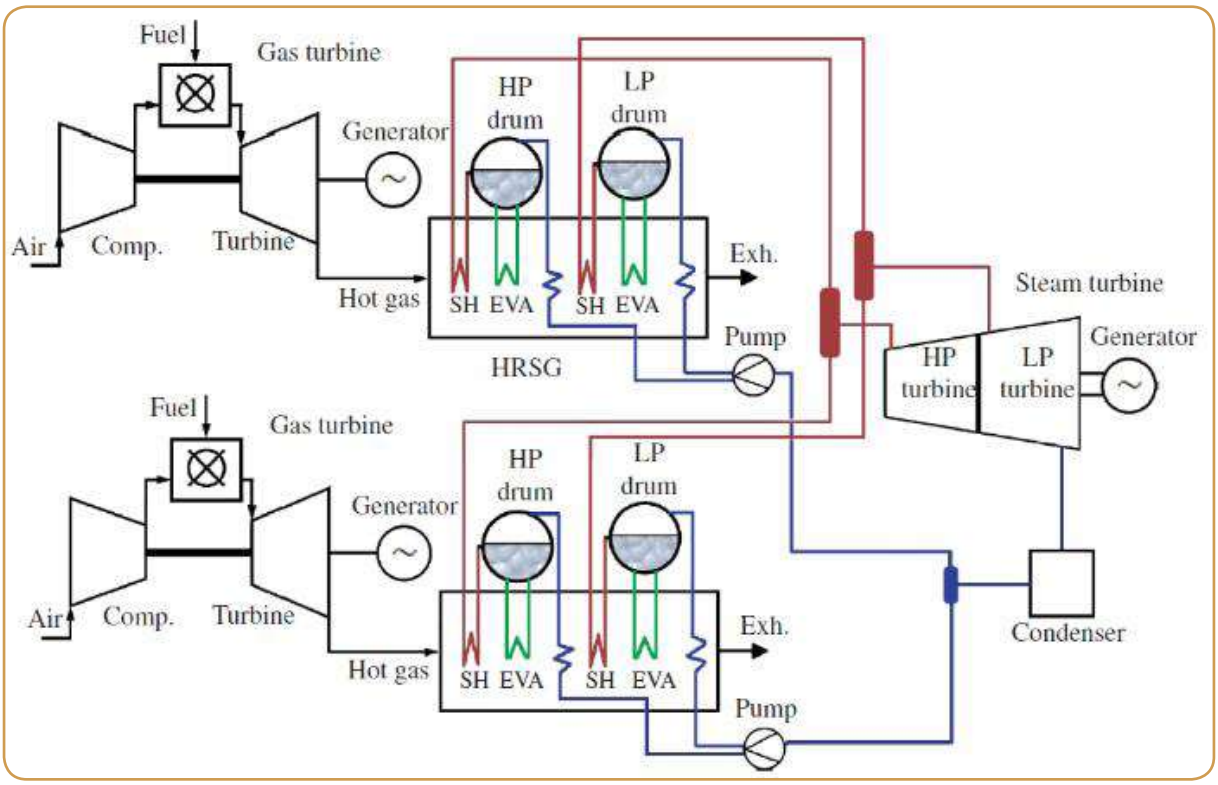

Fig. 1 – Schematic representation of the equipment and assets belonging to the combined cycle power plant unit under investigation

Artificial Intelligent Model

Intelligent Condition Monitoring System (ICMS) is an AI (Artificial Intelligence) model developed by the digitalization group of MAPNA Electric & Control Company (MECO) which enables the experts to identify any degradation in the performance of the related equipment utilizing different graphs and plots.

Key Performance Indicators (KPIs)

Since the studied fault had occurred in the HRSG, its effect on the steam turbine as well as the HRSG's KPIs was investigated. To evaluate the performance of the HRSG, its effectiveness was defined and used using the following equation:

$$\varepsilon = \frac{T_{in,HRSG} - T_{out,stack}}{T_{in,HRSG} - T_{amb}}$$

High pressure section isentropic efficiency of the steam turbine was used for assessment of its performance, as follows:

$$\eta_{isen} = \frac{h_{in} - h_{out,act}}{h_{in} - h_{out,isen}}$$

The above KPI determines the deviation of the actual performance of the steam turbine from its corresponding ideal isentropic performance.

Results & Discussion

After 5 months of analysis, the daily performance trend of the combined cycle power plant unit had been obtained, as illustrated in Fig. 2. Each day, the amount of degraded performance was demonstrated as the percentage of the entire data during the day on which the asset was not in a healthy condition.

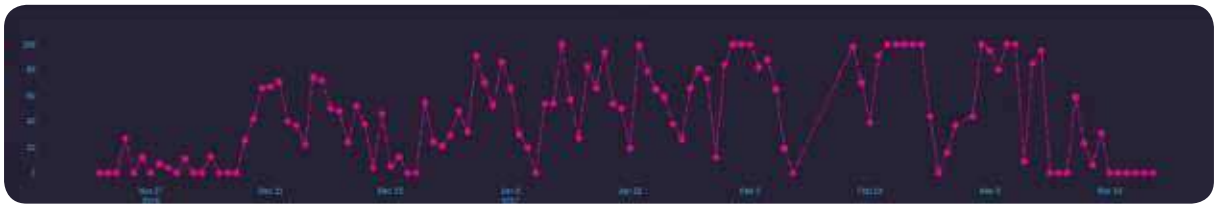

Fig. 2 – Trend of daily performance, horizontal and vertical axes indicate date and percentage, respectively

As it can be seen from Fig. 2, on a couple of days after beginning of the analysis, the degraded performance varies between 0 and 30%, but after Dec. 8th, 2016, the performance curve shows a different pattern in which, unlike the previous days, it does not return to the healthy condition for a long time. The cause of degradation was attributed to the reduced steam temperature at the inlet of the steam turbine's stop valve.

Fig. 3 represents distribution of the inlet steam temperature at the stop valve on different days. Further analysis of the figures indicates that performance degradation had increased considerably in an almost two-month period. In Fig. 3, the horizontal and vertical axes indicate temperature and number of samples taken, respectively. The blue and red regions refer to healthy and degraded performance conditions, respectively.

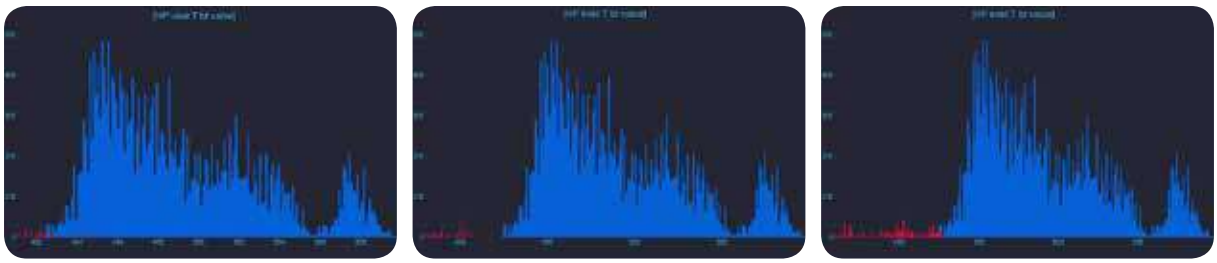

Fig. 3 – Distribution of steam temperature at the inlet of the steam turbine's stop valve; on Dec. 12th, 2016 (left), on Jan. 8th, 2017 (center), on Feb. 7th, 2017 (right)

3D representations of the acquired data are also presented in Fig. 4.

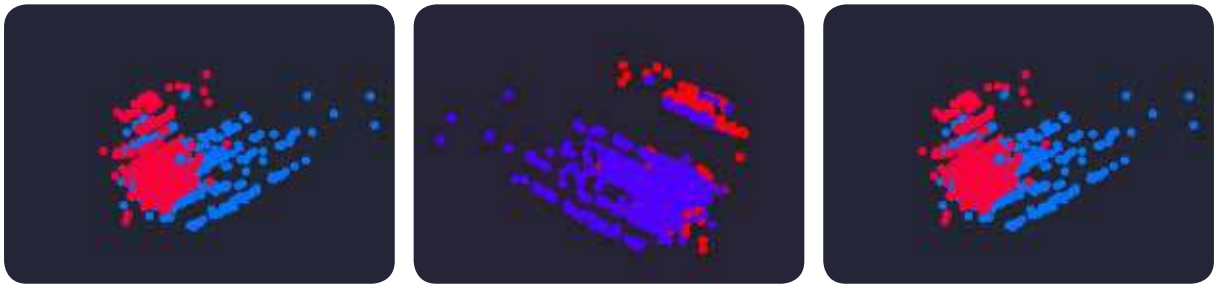

Fig. 4 – 3D representation of the data provided in Fig. 3

Analyzing the data provided in Figs. 3 & 4, it is inferred that the source of the fault could be at the upstream of the steam turbine's stop valve, which had in turn led to temperature reduction at the inlet of the steam turbine. In order to identify the source of performance degradation, the performance of the HRSG was also investigated.

The performance trend of the HRSG demonstrated that, unlike the steam turbine, degradations are up to 100% of the time since the first day of the analysis. Also, it can be seen that the HRSG exhibited degraded performance since Nov. 5th, 2016, approximately one month earlier than the steam turbine degradation symptoms first showed up.

It was shown that the steam temperature at the HP desuperheater outlet of the HRSG was the main culprit for the deviation from healthy performance conditions. Fig. 5 shows distribution of the steam temperature at the HP desuperheater outlet on several days. It demonstrates a trend similar to the temperature at the steam turbine's inlet in a way that it gradually deviates from healthy conditions.

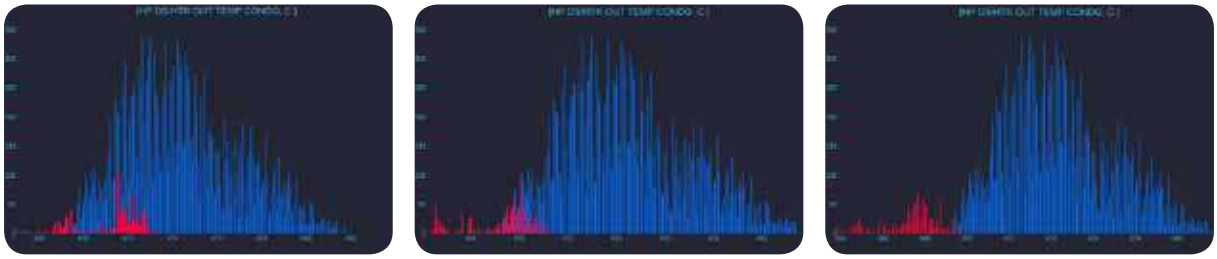

Fig. 5 – Distribution of steam temperature at the outlet of the HRSG's HP desuperheater; on Nov. 24th, 2016 (left), on Dec. 8th, 2016 (center), on Dec. 15th, 2016 (right)

Careful analysis of the list of repair and maintenance activities performed on the studied power plant revealed that in the period between Feb. 21st to Mar. 12th, 2017, a passing of water in the spray valve of the HP desuperheater had been reported and eventually repaired. It described the fault as the inability of the spray valve to close completely despite receiving the close command, which had led to the passing of water into the steam flow, resulting in the reduction of the steam temperature up to 10 °C at the inlet of the steam turbine. It completely conforms to the degraded performance observed in the steam turbine and HRSG. As it is obvious in the performance degradation curve presented for the temperature of the steam at the inlet of the steam turbine's stop valve in Fig. 2, degradation vanished from Mar. 12th, 2017 onward which marks the finishing date of the repairs carried out on the faulty spray valve. From this day on and for the sparse degraded performance incidents observed since, the steam temperature at the turbine's inlet was never listed as the contributing factor for performance degradation.

Fig. 6 demonstrates distribution of the steam temperature at the inlet of the steam turbine's

stop valve on Mar. 25th, 2017. As shown, the distribution had returned to the healthy region, implying the conformity between the analyses performed and the list of repairs made on the power plant unit under investigation.

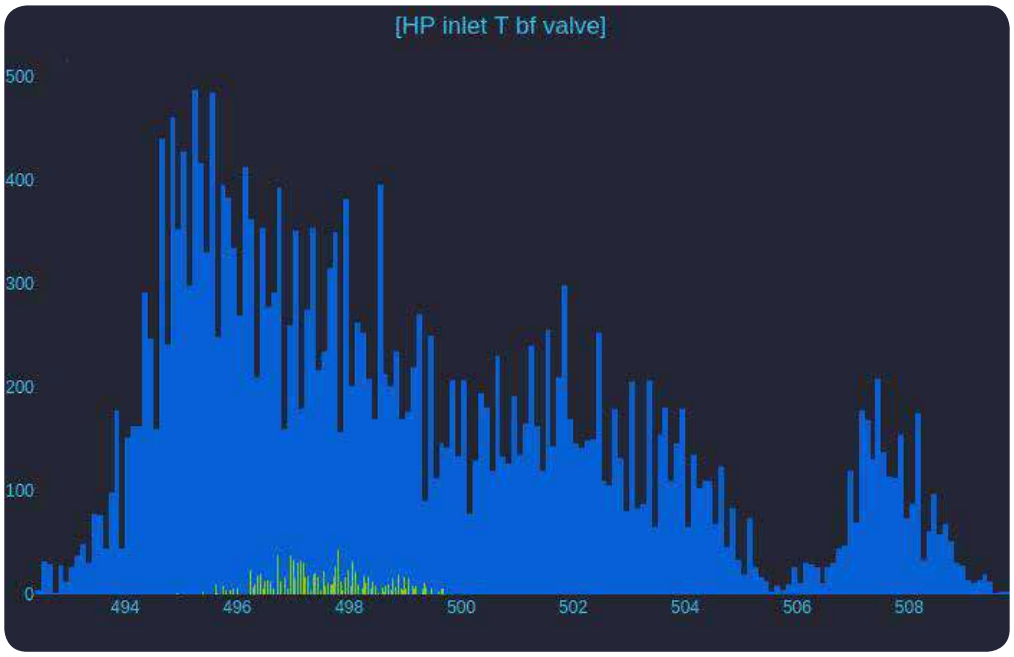

Fig. 6 – Distribution of steam temperature at the inlet of the steam turbine's stop valve on Mar. 25th, 2017 following the repairs made on the faulty spray valve of the HRSG's HP desuperheater

The surprising fact is that temperature reduction and its cause had been identified almost 96 days earlier than it was recorded in the power plant's log sheets. During this period, the deviation grew larger, and once reaching a specific amount, it was identified in the power plant. Another result of the analysis was that by approaching to Feb. 21st, 2017, which was when the repair of the faulty spray valve commenced, power generation of the steam turbine reaches the top on the list of degraded parameters, overtaking the temperature at the inlet of the steam turbine's stop valve. So, it would have definitely been possible to stop such a degrading trend by identification of the symptoms at the onset of their initiation and development, had the ICMS been in place and the faulty valve been repaired earlier.

To analyze the effect of the passing of water in the faulty spray valve of the HP desuperheater on HRSG and steam turbine KPIs, HRSG's effectiveness and steam turbine's isentropic efficiency trends are shown in Figs. 7 & 8, respectively. As demonstrated, the effectiveness of the HRSG drops about 3% prior to initiation of the repair activities and then returns to its healthy condition after Mar. 12th, 2017. It is clear that the reduction of the HRSG's effectiveness is small at the early stages of the fault identification using ICMS.

The trend of the isentropic efficiency of the steam turbine is shown in Fig. 8. As expected, the reduction of steam temperature at the inlet of the steam turbine leads to decreased turbine efficiency. A reduction of 8% had been observed due to the valve leakage, which recovered following the implementation of repair activities. As was the case with the HRSG, the decreased efficiency of the steam turbine was also small at the time of fault identification by ICMS.

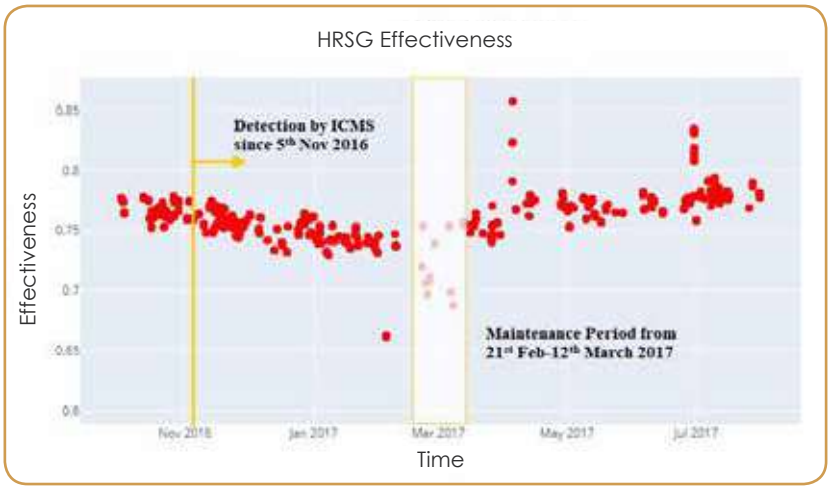

Fig. 7 – HRSG effectiveness trend

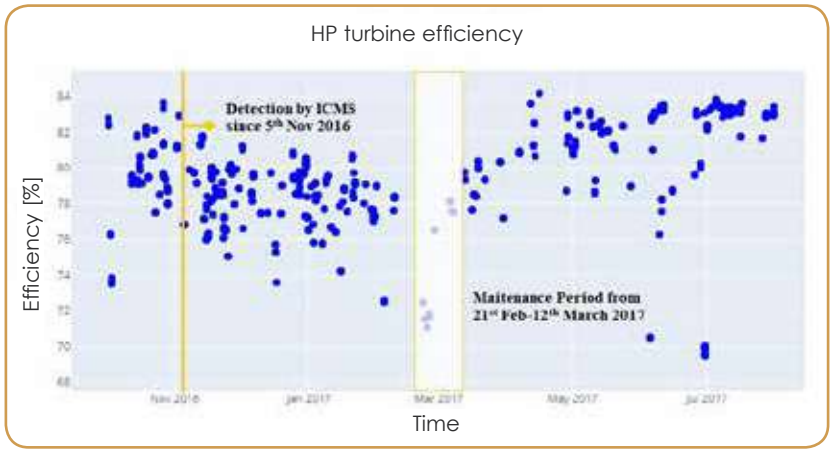

Fig. 8 – HP steam turbine's isentropic efficiency trend

Concluding Remarks

In the present article, a case study was performed on a fault within the HRSG of a combined cycle power plant unit, and its effect on the steam turbine performance was investigated. An artificial intelligence model was used to detect the fault. The intelligent condition monitoring system (ICMS) used for this investigation was based on an Artificial Intelligence (AI) model developed by MAPNA Electric & Control Company (MECO) digitalization team. The model was used to identify degraded performance of the steam turbine and HRSG. It was demonstrated that the reduced steam temperature at the inlet of the steam turbine's stop valve had led to the deviation of temperature distribution from normal healthy conditions. It was observed that this reduction was the result of the excessive decrease in the steam temperature at the HRSG's HP desuperheater outlet. It was shown that this temperature reduction led to about 3% decrease in the HRSG's effectiveness and 8% decrease in the isentropic efficiency of the steam turbine.

Careful analysis of the list of repairs and maintenance activities performed on the studied power plant unit revealed that a repair had been done on the spray valve of the HRSG's HP desuperheater due to the leakage of water into the steam flow despite receiving the close command. The restoration of the steam turbine performance to healthy condition was exactly in coordination with the ending date of the repairs implying the accuracy of the model in identification of degraded conditions encountered. It would have been readily possible to identify the fault 96 days earlier than the date on which it was first showed up in power plant's log sheets.

2

First MGT-30 Gas Turbine Additively Manufactured Part Set To Render Conventional Manufacturing Process of the Part Obsolete

Fathi, Alborz
Ghodsi, Mahsa
Davarzani, Hossein
Vatanara, Masoud

MAPNA Turbine Engineering & Manufacturing Co. (TUGA)

Introduction

The first step to integrate an additive manufacturing process in the production lines of a product is to get a comprehensive view on the whole process chain. It is far more important for metal powder bed processes such as SLM[1] specially when applied on critical components of a turbomachine.

Due to some technical issues and following a comprehensive risk analysis, fixing device which is a part of the MGT-30 gas turbine combustion chamber, was chosen as the first turbine part to be produced in MAPNA Turbine additive manufacturing laboratory.

Due to its relatively simple design, the main challenge of additively manufacturing this part was to develop the powder, process and heat treatment parameters to achieve the acceptable physical and mechanical properties of the part.

The statistical approach taken to achieve the optimum properties as well as the whole process chain of the fixing device production is elaborated on in the present article.

[1] Selective Laser Melting

Manufacturing Parameters Optimization

■ Metal Powder

The powder used in the additive manufacturing process shall have some special properties including sphericity, appropriate particle size distribution, low amount of surface impurities and absorbed gases, as well as proper chemical composition. Deviation of these properties from the accepted values would result in improper flowability of the powder or defects in the final product.

The fixing device is made of Inconel 625–a nickel-based superalloy. Therefore an AM grade IN625 powder had to be used for its production. Chemical composition and physical properties of the powder used for this purpose are listed in Tables 1 & 2, respectively.

Table 1 – Chemical composition (weight percentage) of the used AM grade IN625 powder

Element	C	Mn	P	S	Si	Cr	Ni	Mo	Fe	Co	Nb	Ti	Al
Standard (ASTM F3056)[2]	<0.1	<0.50	<0.015	<0.015	<0.50	20.0-23.0	Bal.	8.0-10.0	<5	<1.0	3.15-4.15	<0.4	<0.4
IN625 Powder					0.18	20.88	Bal.	10.25	3.44		4.39		

Table 2 – Physical properties of the used AM grade IN625 powder

Flow Rate (s/50gr)	Apparent Density (gr/cm^3)	PSD (µm)		
		D10	D50	D90
14.6	4.54	25.12	40.48	63.39

■ Laser Parameters

There are more than 100 parameters to be set and controlled to get an acceptable workpiece via the SLM process. One of the most important parameters is the heat density due to its controlling effect on the size, penetration, and turbulence of the melt pool and hence affecting the uniformity of the workpiece surfaces, amount of residual stresses, dimensional tolerances, microstructure as well as size and shape of the defects. Heat density is a function of the three following items:

- Laser Power
- Scan Speed
- Scan Strategy

Briefly, increasing the laser power and decreasing the scan speed will lead to the enlargement of the melt pool. However, each of these parameters has a separate effect and if adjusted improperly, it would bring about some defects like lack of penetration, spattering, or balling. Besides, during the scanning of the whole surface, some other parameters such as melt pool overlaps and moving path of the laser beam are also important. Scanning strategy describes all the parameters to determine how to move the laser point on the powder bed to scan the whole selected area. Scanning strategy mainly affects residual stress and final surface

roughness of the part. It is obvious that all these parameters have strong correlations with each other to produce a smooth, intact area in each individual layer as well as in between adjacent layers.

There are several ways to get an optimized set of parameters. In general, one standard algorithm is to produce a qualified single line, then a qualified single surface, and finally a qualified specific volume. Subsequently, the accepted parameters set shall be modified for different divisions of the surface, border, support, and upper surfaces.

In the current investigation, a statistical approach was taken to optimize the manufacturing parameters. It means that the mentioned algorithm was not performed and instead, Design of Experiment (DOE) methods and taking advantage of commercial statistical software were tried to achieve the best properties directly.

In doing so, the following constants and assumptions were made at the onset of the process:

- The layer thickness is considered to be 30 µm
- Since the surface of the final part will be machined, the border parameters are set identical to the contour parameters. It means that the final surface roughness is not the goal
- The building direction of the fixing devices on the workpiece shall be in a way that can be easily separated from the building platform by a band saw, therefore the support parameters were set identical to the contour parameters in the first step
- A chessboard scan strategy with an optimum square dimension was applied to minimize the residual stresses

Considering these assumptions, the main goal was then to optimize following parameters to minimize the porosity of the final part:

- Laser power
- Scan speed
- Hatch space (Determining the overlap percentage of the melt lines)
- Increasing angle (Specifying melt lines rotation in various layers with a constant angle)

The domain of parameter changes was determined through manufacturing some preliminary metallographic test samples. The hatch space was set so as two adjacent melt lines did not have any overlap and each melt pool section was clearly observed. The microstructures of these samples are shown in Fig. 1 for different power and speed percentage values. From Fig. 1 it is obvious that increasing the heat density (increased power and/or decreased speed), would result in more uniform and larger melt pool size. However, it should be noted that too high heat density may lead to spattering or keyhole effect bringing about defects in the final workpiece. For too low power and too high speed conditions, the heat density was not enough for a rigid test piece to be formed and hence no microstructure was available for such operational conditions. According to the results obtained, the extent of the parameters was set as follows:

- Power: As a continuous factor between 77% to 100%
- Scan speed: As a continuous factor between 50% to 75%
- Hatch Space: As a continuous factor between 23% to 57%
- Increasing angle: As a categorical factor between 0 and 1 (whether the melt line orientation does or does not rotate in various layers)

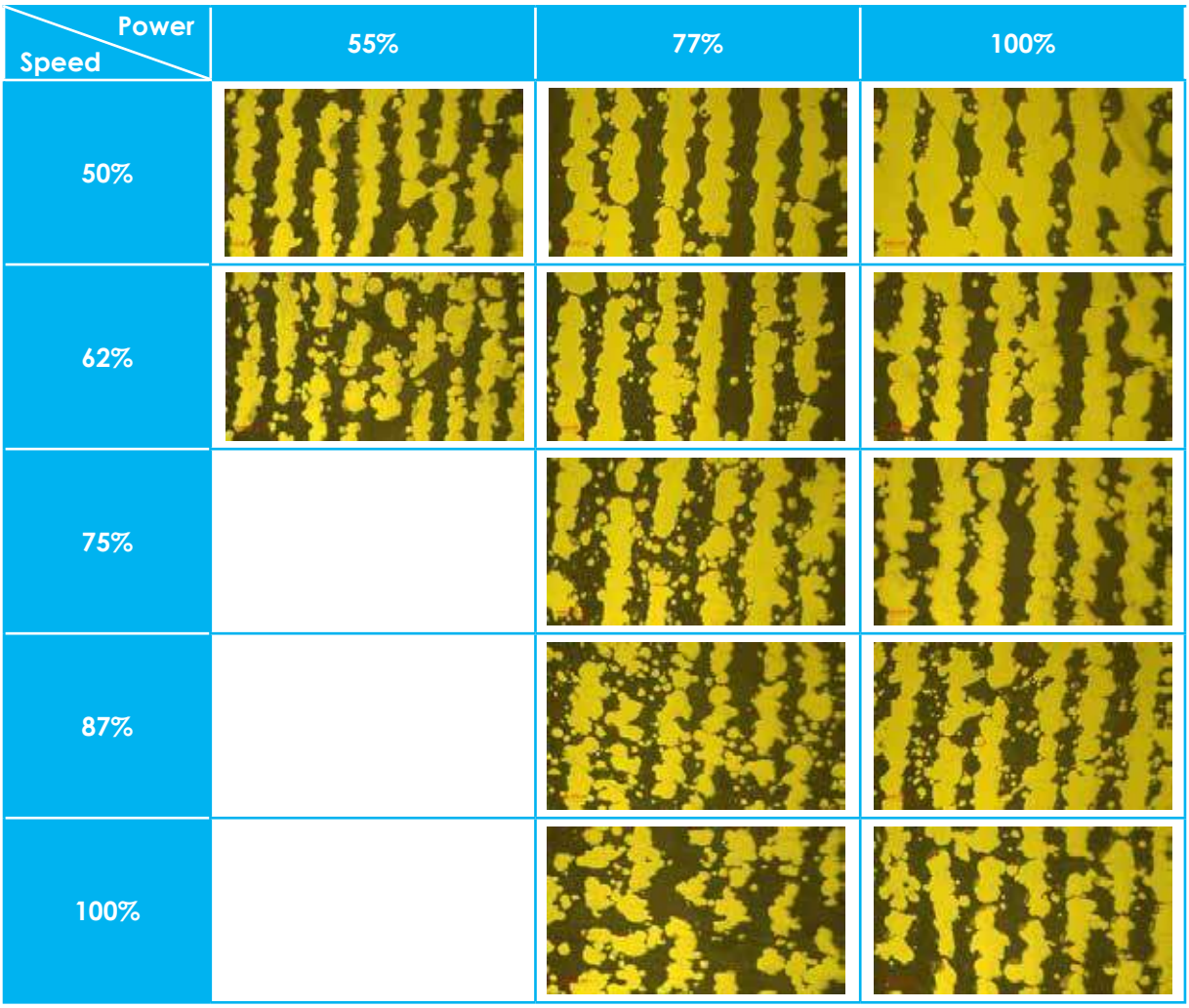

Fig. 1 – Optical microscopic images of the microstructures of the additively manufactured test specimens for different (dimensionless) power & speed values

Commercial statistical software was used to design the main tests. Due to some limitations in test conditions, BBD[2] method with 6 central points was applied to design 30 set parameters. Several cross-sectional areas were observed using optical microscopy to evaluate the porosity percentage of each specimen. Fig. 2 represents the correlation between the heat density and the porosity percentage. As expected, increasing the heat density results in the reduction of the porosity percentage dealt with.

Following some careful analyses an optimized relation between the working parameters and porosity was established bringing about minimized porosity percentage.

As a final step and to check the final results, a sample specimen was manufactured. The porosity percentage was measured to be less than 0.2% and deemed to be a very good result referenced to the literature [3,4].

[2] Box-Behnken Design

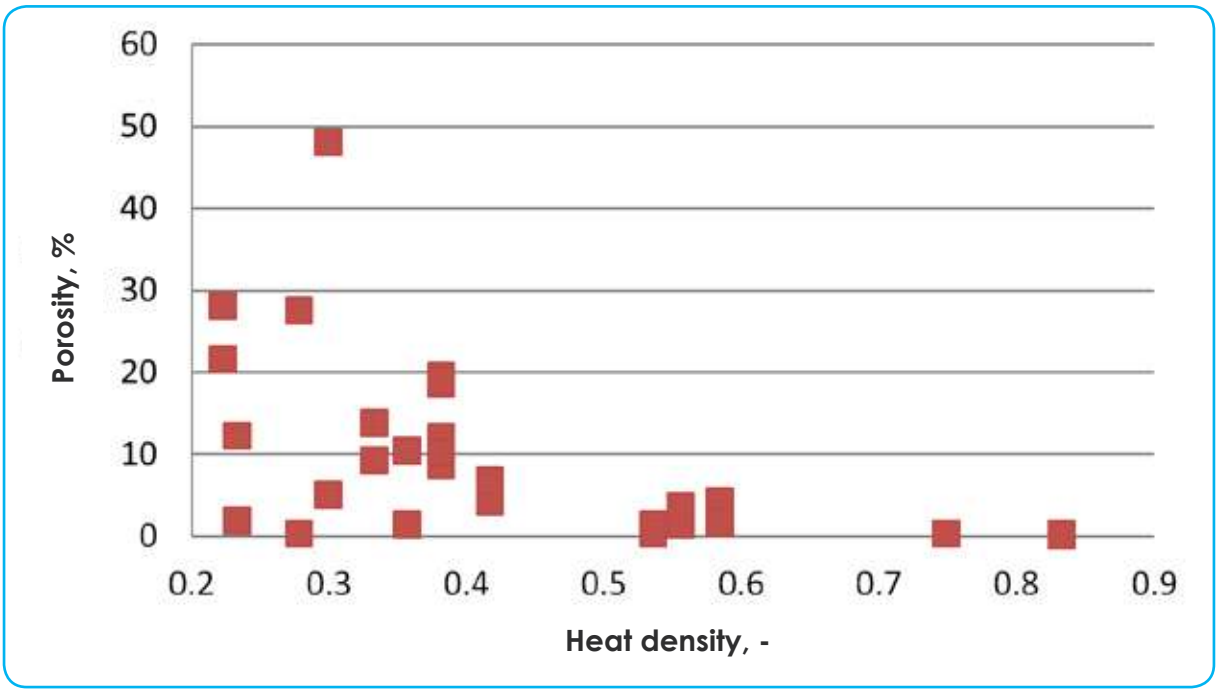

Fig. 2 – Porosity percentage versus heat density (dimensionless) for the tested specimens

■ Heat Treatment

Thermal cycles during the SLM process would result in increased residual stresses and microstructural inhomogeneity of the manufactured part. In some instances, if the supporting step is not performed correctly, the residual stresses may lead to the failure of the process before it is finished. But even if the part is considered acceptable in an as-built condition, the residual stresses are likely to impact the dimensional tolerances or even may lead to deformation of the part. Furthermore, the cast microstructure of the as-built part is not deemed suitable for many in-service applications and the part would still need a microstructural transformation based on its material's nature.

According to ASTM F3056 standard [2], additively manufactured parts made of IN625 must undergo a heat treatment process to release the internal stresses and annealing the cast microstructure in 1038 °C followed by an air quenching.

To evaluate the metallurgical and mechanical properties of the manufactured parts several rods and cubes were manufactured using obtained optimized parameters. Several specimens then underwent a heat treatment process by going through the cycle outlined earlier (Fig. 3).

Fig. 3 – A photo representing heat treatment of the tested specimens (rods & cubes) in action

Microstructural evaluation of the manufactured specimens was carried out prior (as-built) and after going through the specified heat treatment process, as shown in Fig. 4.

Melt pool shape, overlap and dendritic structures are clearly visible in Fig. 4(a). The porosity percentage is also acceptable for both cases. In both specimens, the grains are elongated parallel to the heating direction and perpendicular to the layer surface.

However, following the heat treatment procedure, the structures are entirely different. As it is clear in Fig. 4(b), the layer boundaries as well as all the dendrites are disappeared and a homogenous annealed structure is provided.

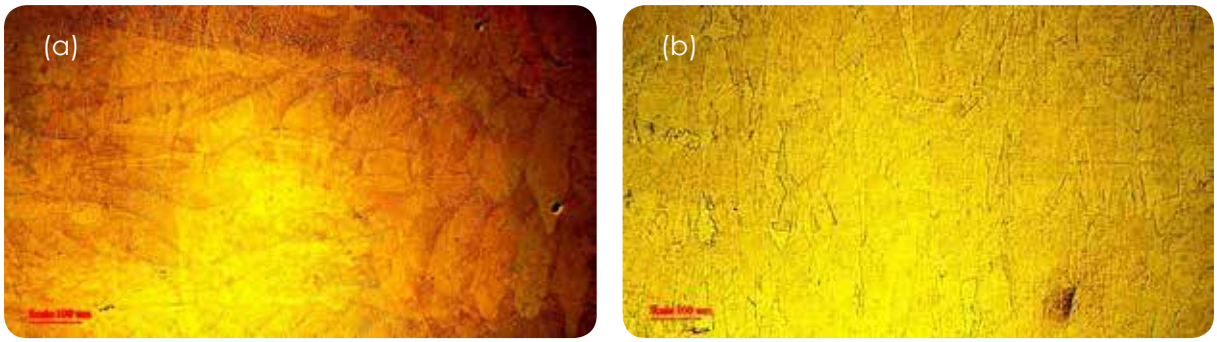

Fig. 4 – Microstructure of the as-built (a) & heat-treated (b) AM specimens

The results of strength analyses performed on rod specimens of different statuses and origin are listed in Table 3. As it is evident in Table 3, yield stress and tensile strength values of the additively manufactured specimens are way above those of standard-cited and conventional material values for both as-built and heat treated specimens. However, the elongation percentage shows a substantial improvement for the heat treated specimens by closing in on to the standard-cited acceptance criteria.

Table 3 – Results of strength analyses performed on rod specimens of different statuses

Status	Yield Stress (MPa)	Tensile Stress (MPa)	Elongation (%)	Hardness (HV)
As-built	762	976	22	312
Heat-treated	604	879	29.5	261
ASTM F3056/Heat-treated [2]	275	485	30	-
Original Part Material	345	785	25	-

Mean hardness values (averaged over 3 points, minimum) are also measured and listed in Table 3. Mean hardness value of the heat-treated specimens is deemed acceptable in comparison with the original material properties of the fixing device. So, it can be concluded that applying approved heat treatment cycle would lead to acceptable properties for the additively manufactured fixing device part to ensure a safe and reliable operation under actual service conditions.

Fixing Device Manufacturing Process Chain

■ Pre-process

Production of the fixing device started with a primary model. Based on the final machining and service conditions as well as dimensional and geometrical tolerances, some changes were applied to the model. In the next step, the position of the part on the manufacturing

platform was finalized. The position of the part and manufacturing direction would have a significant impact on the manufacturing time, surface quality, and tolerances. In the last step of the modeling procedure, supporting and layering were performed. Fig. 5(a) shows a 3D representation of the fixing device model at the end of this step.

To evaluate residual stresses and to approve the supporting step, process simulations were also performed on the model, as shown in Fig. 5(b). According to the results, the amount of residual stresses and stress concentration points were acceptable implying the adequacy of the support type and volume.

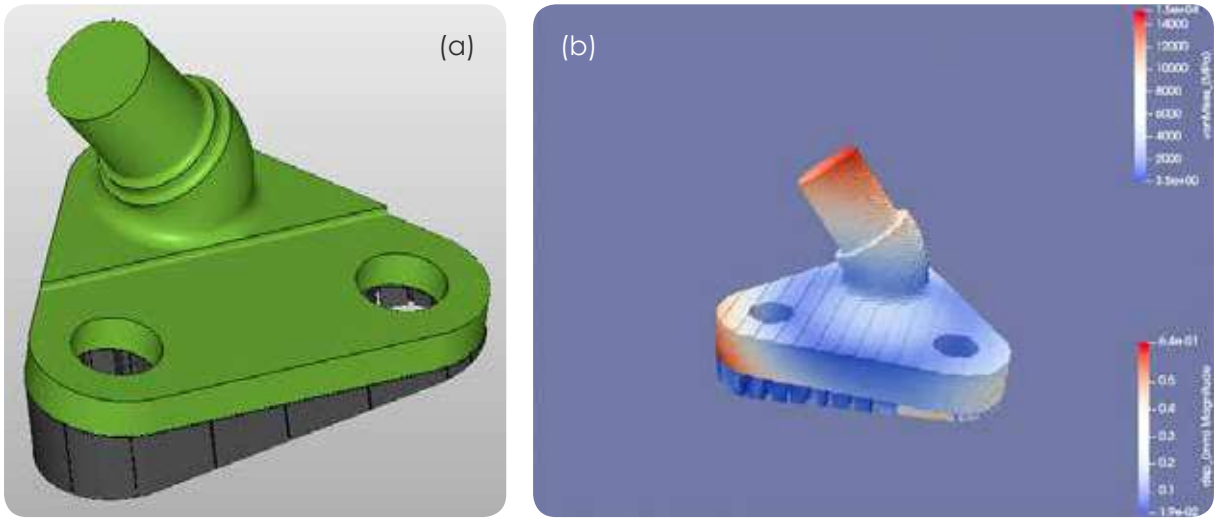

Fig. 5 – 3D model of the fixing device supported (left) & simulated (right)

■ Manufacturing Process

Three approved prototype models were located on the manufacturing platform, as shown in Fig.6. It is to be noted that, for investigation of the fixing device performance under actual service conditions, only a limited number of prototypes were manufactured following implementation of rigorous qualification tests. In the case of mass production, appropriate qualification tests shall be designed for all pertinent production steps.

The approved manufacturing parameters applied to the parts and after preparing the SLM machine and atmosphere the SLM process was started. It took 16 hours of operation for the 3 prototype models to be manufactured. Fig. 6(b) shows a photo of the additively manufactured parts upon completion of the SLM process.

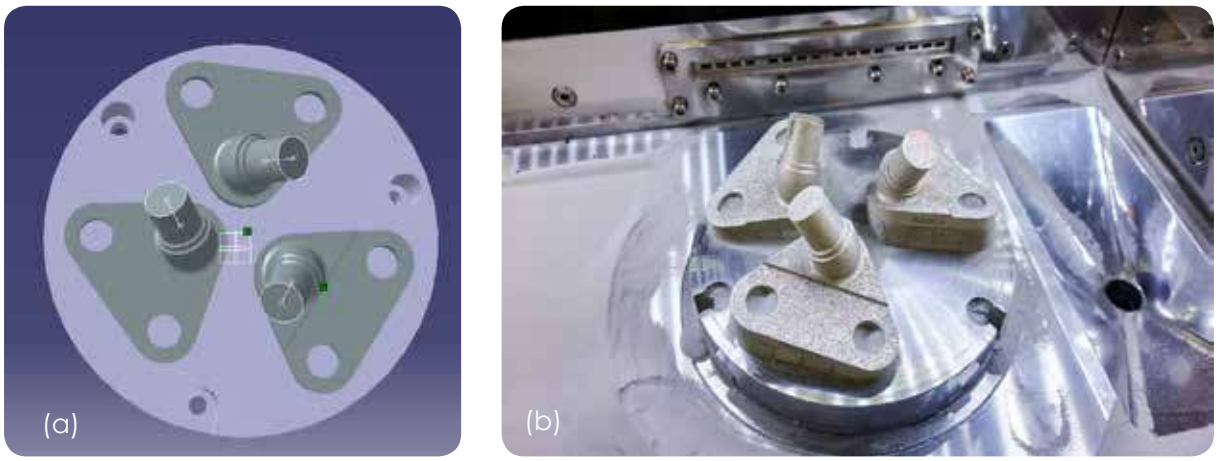

Fig. 6 – A view of fixing device prototype models put on the manufacturing platform of the SLM machine (a); A photo representing additively manufactured parts (b)

■ Post-process

Heat treatment using approved cycle was performed on the prototypes. Due to the residual stresses within the manufactured parts this process shall be done prior to the removal of the support.

Support removal was carried out by EDM and according to the production routine. Following steps were taken for the manufactured parts:

- Hard facing via welding
- Stress relief heat treatment
- Final machining

■ Inspection & Qualification

Following inspection & qualification tests and analyses were performed on the manufactured parts with satisfactory results:

- Dimensional check to evaluate the deformation
- Visual check
- Penetrant test
- Radiographic test

Costs & Benefits

Relatively simple design of fixing device causes small benefits from this point of view. But even in this situation, manufacturing via SLM method provides a number of benefits summarized as follows:

- A reliable production method of the fixing device can help to progress according to the organizational production plan in critical time periods. The additively manufactured parts with the minimum lead time would be a perfect choice for replacement of the rejected low quality parts manufactured with routine casting or machining process.
- In comparison with other fixing devices, a near net-shape AM fixing device needs around 45 hours less machining time in the production chain.
- The final cost depends on the number of the order. But in case of a single set order the manufacturing cost will be reduced by about 40% compared with the round bar machining process.

Current In-service Status of the Prototype Models

Final qualification assessment of the prototype models is currently under way through condition monitoring of the parts performing in actual service conditions. The AM fixing device prototypes assembled on an MGT-30 gas turbine, shown in Fig. 7, have successfully reached a record 3500 EOH so far without any report of defect or improper operation. These parts will be checked and controlled in specific periods of time to evaluate the condition and life of the AM fixing devices during their service lifetime.

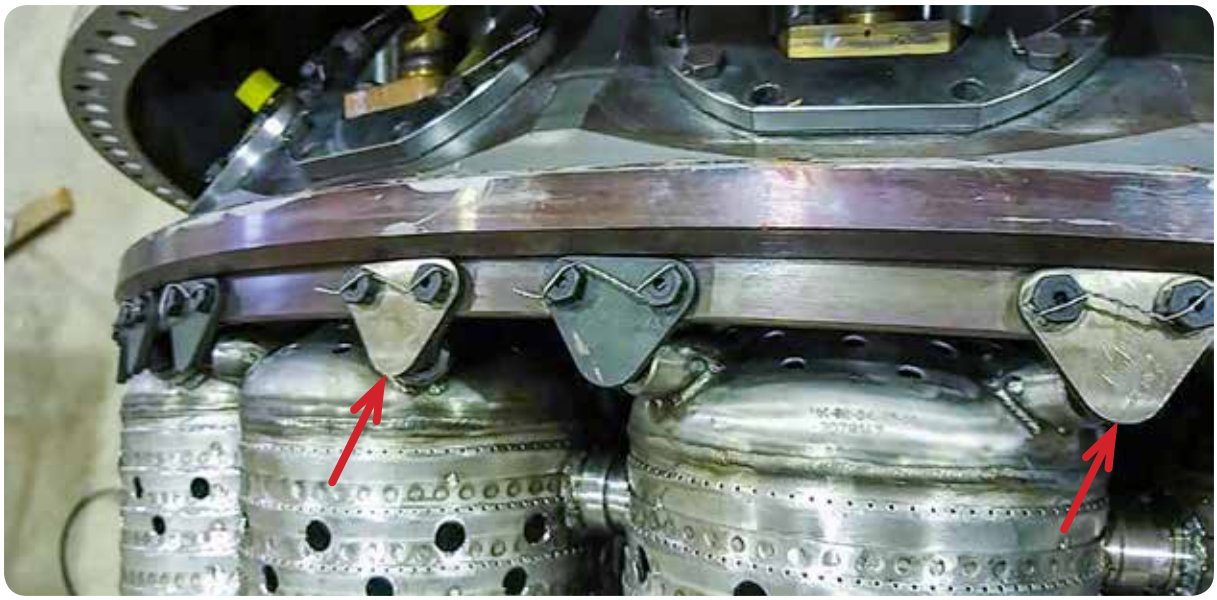

Fig. 7 – A photo indicating AM fixing device prototypes assembled on an MGT-30 gas turbine, undergoing actual service conditions test runs

References

[1] "Wohlers Report 2018: 3D Printing and Additive Manufacturing State of the Industry Annual Worldwide Progress Report", *Wohlers Associates*, 2019.

[2] "ASTM F3056: Specification For Additive Manufacturing Nickel Alloy (UNS N06625) With Powder Bed Fusion", 2014.

[3] I. Koutiri, E. Pessard, P. Peyre, O. Amlou, T. De Terris, "Influence of SLM process parameters on the surface finish, porosity rate and fatigue behavior of as-built Inconel 625 parts", *Journal of Materials Processing Technology*, Vol. 225, PP. 536-46, 2018.

[4] M.Salarian, H.Asgari M.Vlasea, "Pore Space Characteristics And Corresponding Effect On Tensile Properties Of Inconel 625 Fabricated Via Laser Powder Bed Fusion", *Materials Science & Engineering: A,* Vol. 769, 2020.

3

A New Ultrasonic Method for In-Service Inspection of Gas Turbine Vane Tenons

Kiyanmanesh, Mohammadreza
Moradkhani, Sadegh
Ahmadian, Hossein
Vatanara, Masoud

MAPNA Turbine Engineering & Manufacturing Co. (TUGA)

Introduction

Turbine problems and equipment failures are primary causes of power plant outages leading to costly maintenance and repair procedures.

Typically, a gas turbine compressor includes multiple stages or rows/rings of vanes along the turbine shaft. Most of these rings are structurally stabilized by inclusion of a circumferential structural band, or shroud, interconnecting all or a group of the vanes at the outer tips of the vanes.

Tenon is an extension of a turbine vane which is shaped so as to fit into an opening in the shroud making it difficult for an inspection to be carried out. While in operation, high rotational speeds, vibration and temperature changes can combine to produce significant stresses in turbine wheels, and particularly in the vanes' tenons affixed to the shrouds. Material losses, and failures of tenons, are some of the most common problems encountered with gas turbine operation. A tenon may initially have or later on develop a very small crack or undergo a thickness reduction which, under operating stresses, would result in complete fracture. This would increase the stresses applied on the tenons of the adjacent vanes, which in turn can lead to more fractures, worsening the situation by further increasing the stresses applied on the other tenons.

The corresponding shroud segment will finally have nothing to hold it tight in its place and following an array of breaks at high rotational speed, the turbine will eventually suffer seriously from internal damages. It may result in unscheduled outages which could last from several days to months, entailing exorbitant repair costs to a power plant.

Tenon failure can be avoided via timely inspections to provide early detection of faults or cracks while they are still too small to impair the structural integrity of the components. A serious impediment to effective inspection is that the most likely location for an initial fault is in the turbine vane tenons at the point where it is fixed to the inside surface of the circumferential shroud, a point which is highly inaccessible in the assembled turbine rings. Inspections following disassembly of the

components are also costly, time consuming and possibly destructive for the tenons, since the welded shroud must be removed, limiting the reusability of the shroud.

In the MGT-70 gas turbine, there are 16 stages of stationary compressor blade rings placed into the outer shell of the gas turbine; three of them are displayed in Fig. 1. All compressor stages have different dimensions reducing in size from the 1st stage to the 16th stage. At each stage, the blade's tenon is placed between two inner rings as can be seen in Fig. 2. All tenon locations shall be tested without disassembly of the upper and lower rings during a turbine overhaul. A photo representing defective tenons following disassembly of the rings is also shown in Fig. 3. The most prevailing defect is thinning of the tenon in the location between the airfoil and the shroud as illustrated in Fig. 3.

Fig. 1 – Upper and lower rings of MGT-70 gas turbine compressor stationary blades

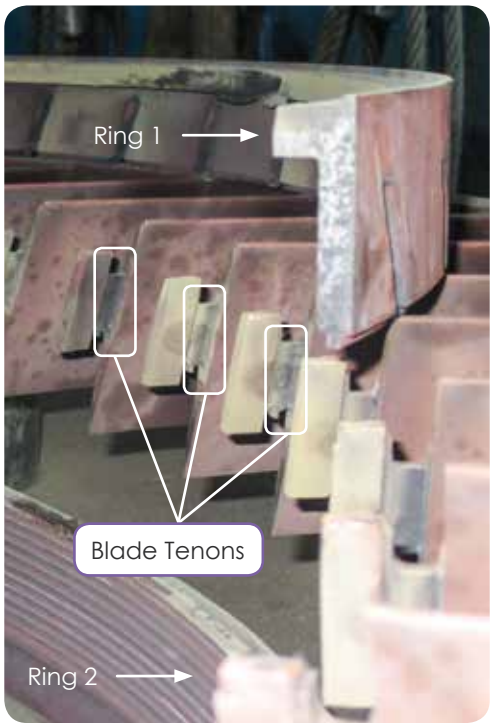

Fig. 2 – Stationary compressor blade tenons following disassembly of the lower (Ring #1) and upper (Ring #2) rings

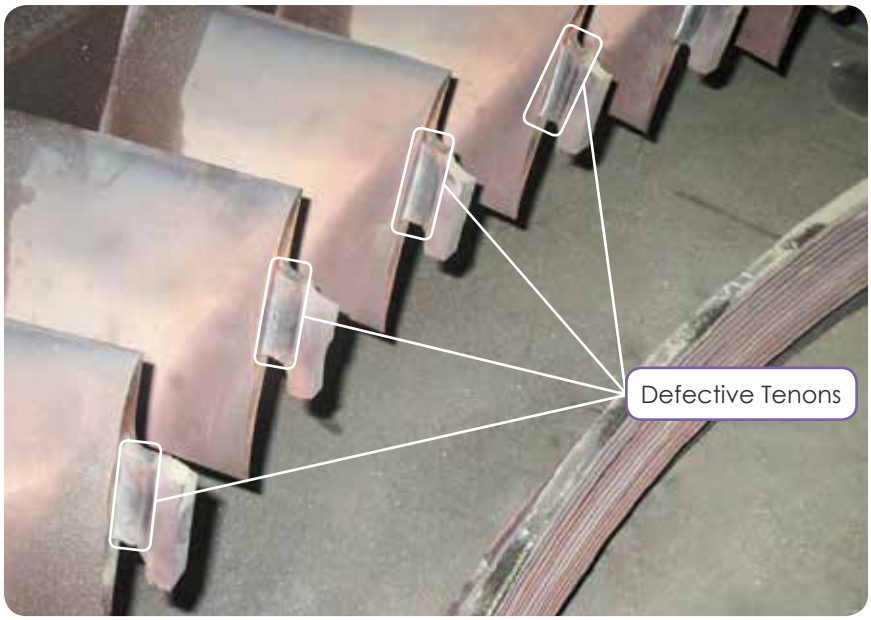

Fig. 3 – Defective tenons exhibited following disassembly of the lower and upper rings

In this article, an innovative inspection method specifically developed to assess the condition of MGT-70 gas turbine compressor vane tenons is outlined and elaborated on.

Methodology

Ultrasonic waves can travel in different modes commonly including: longitudinal (compression), shear (transverse), surface (Rayleigh) and plate (lamb) modes.

■ Wave Properties

Longitudinal waves are the ones in which the direction of particle vibrations is in the back and front of the direction of the wave propagation. In contrast, the direction of particle vibrations in shear waves is perpendicular to the direction of the wave motion.

Moreover, shear waves could not travel through liquids or gasses. In some materials, the velocity of a shear wave is about half that of the longitudinal waves.

Surface-beam Rayleigh waves travel at an angle of 90° to the normal vector of the examination surface. In materials with thicknesses of more than double of the wavelength, the Rayleigh wave can penetrate to a depth of approximately one wavelength regarding its potential energy. Meanwhile, one half of its energy is within one-quarter wavelength of the surface due to the exponential distribution of the energy.

Lamb waves travel at an angle of 90° to the normal vector of the test surface and fill through the bulk of thin materials because of their elliptical particle vibrations. These vibrations occur in various layers and travel at velocities slower than the Rayleigh waves and closer to the longitudinal waves depending on the material thickness and examination frequency.

■ Test Equipment

In this investigation, following testing equipment were used:

Table 1 – Used test equipment

Flaw detector	Ultrasonic flaw detector Epoch XT
Transducers	Shear wave probe: Angle 45 to 70°, Size 7*10, Frequency 2~5 MHz
	Surface wave probe: Angle 27.5°, Size 8*9, Frequency 2~5 MHz
Couplant	Lubricating grease

■ Preparation of Test Specimens

After measuring the thicknesses and shapes of the vanes of all 16 compressor stages, the vanes of two stages were chosen to be used as test samples. The simulations carried out, showed that the thickness and curvature of all compressor stages are covered by just two stages of 4 & 13. Since the procedure will be done during an overhaul, defect-free test samples extracted from a gas turbine compressor were used for the experiments as shown in Fig. 4.

Fig. 4 – MGT-70 gas turbine's 4th (left) and 13th (right) stage stationery compressor blades used in the evaluation of capability and sensitivity of defect detection methods

Moreover, two step-wedge test blocks (with 0.1, 0.2, 0.3, 0.4, and 0.5 mm steps) with the same material and thickness of the corresponding compressor vanes were built, as shown in Fig. 5, to evaluate the sensitivity of the developed flaw detection method using shear and surface wave transducers.

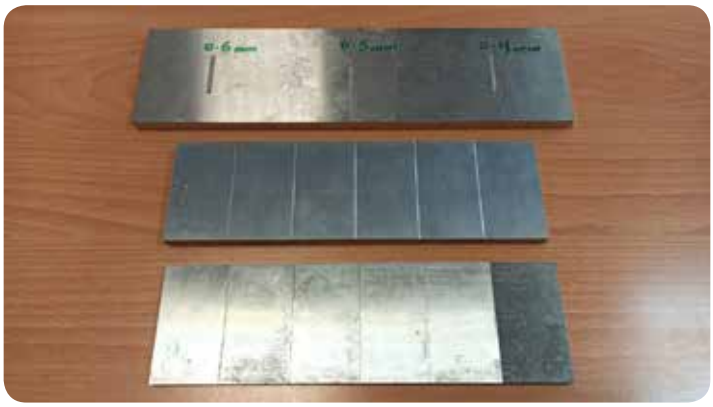

Fig. 5 – Step-wedge test blocks used for the sensitivity analysis of the developed defect detection method

Finally, an overhauled gas turbine compressor ring with some notches of different sizes made on the suction (convex) side of some of its vane tenons was used to evaluate the accuracy of the developed procedure in a completely assembled set of vanes, as shown in Fig. 6.

Fig. 6 – Test setting preparation for the evaluation of the developed defect detection method

■ Calibration

The ultrasonic pulse-echo instrument was calibrated using a V2 standard calibration block (based on ASME Sec.5). Sensitivity calibration of shear and surface wave probes with two sets of vanes (stages 4 & 13) and step-wedge blocks were performed, respectively. Doing so, detection of the maximum back wall reflection from the convex side of the vanes of the stages 4 and 13 was performed using shear wave probes, as shown in Fig. 7. Afterwards, the optimum back wall's echo amplitude was adjusted on 100% FSH (full screen height) and the time-based linearity was recorded. The surface wave probe sensitivity was also determined using step-wedge blocks and testing data was set for detecting induced defects in the demonstration test performed.

Fig. 7 – Calibration of shear wave probes on individual compressor vanes

Results & Discussion

The shear probe was placed on the suction side of the compressor vanes (demonstration test). Results revealed that in all defective vanes, defect's echo arrived between the initial pulse and back wall echo implying the presence of a discontinuity in the tenon area, as represented in Fig. 8. Moreover, the surface wave probe provided the same results in a shorter time frame and accurately identified all defective vanes.

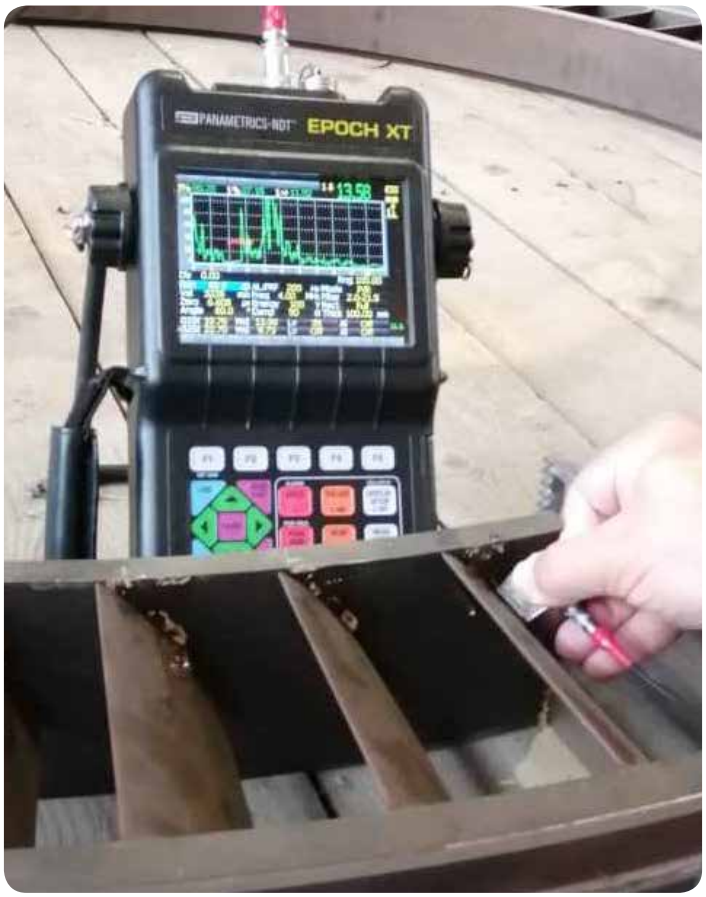

Fig. 8 – Demonstration test of the developed defect detection method on an assembled array of stationery compressor blades

Concluding Remarks

Experimental investigations demonstrated that a pulse-echo ultrasonic testing method to detect thickness reduction of compressor vane tenons using two types of probes is beneficial to in situ inspection of compressor vane tenons eliminating time consuming and destructive gas turbine compressor vanes' disassembly. Material losses as small as 0.5 mm deep were detected successfully. This experiment proved that surface wave testing offers more favorable speed, sensitivity, and simplicity of use compared to shear wave probes. All in all, MAPNA Turbine once again succeeded to develop and apply a specialized non-destructive test method for improving reliability of their gas turbine products. The developed method will bring about broader applications in the future by providing low cost inspection and maintenance services.

4

Successful Development of a Scoop Sampling Device

Soheili, Masumeh
Vatanara, Masoud
Khodabakhshi, Meisam

MAPNA Turbine Engineering & Manufacturing Co. (TUGA)

Introduction

Critical components of power plants operate under severe conditions of high temperatures and pressures for long periods of time. Long-term exposure to such harsh conditions brings about degradation of the microstructure and deterioration of material properties.

Deterioration of material properties leads to significant drops in power equipment performance and durability. In order to maintain the operating integrity and reliability of the power equipment, it is highly necessary to keep track of potential damage mechanisms which could take place during operation as well as estimate the state of the damage incurred or life consumption of the components as accurately as possible. Mechanical properties assessment of in-service components is also vital to estimate safe remaining service life of the components. This could be done via standard tests which are generally hindered by the limited amount of material that could be extracted from the components. This has led to further development of non-destructive and semi-destructive test methods. Scoop sampling is a semi-destructive specimen extraction method which makes small-size samples of the corresponding material available for further analyses of in-service components.

Scoop Sampler Machine

The most accurate way for determining an aged material's condition is through destructive testing. For a large plant component, sampling is necessary. Without additional care, sampling could lead to increased stress concentration, reduced wall thickness and diminished service life of a component. Scoop sampling machine is designed to operate in such a way that no changes are made in the mechanical and metallurgical properties of the corresponding material.

The following criteria are important in designing a scoop sampling machine:

Weight: For increased maneuverability in sampling of in-service components and for comfortable handling and easy transport, it should be as light as it could possibly be.

Set up: It must be easy to set up on any curved or flat surfaces and parts' corners for in-service components sampling.

Scoop dimension: As per required test specimens' dimensions, the scooped sample's dimension is to be 25.4 mm in diameter with a thickness of 4 ± 0.2 mm.

Temperature: While sampling, overheating must be avoided to prevent alterations in the mechanical and metallurgical properties of the material.

Crushing & deformation-free sampling: The sampler cutter must be able to cut out samples without leaving any crushing, pitting and/or deformation on the substrate while maintaining a suitable lifetime.

A photo representing the scoop sampler device designed and developed by Rolls-Royce is shown in Fig. 1.

Fig. 1 – Scoop sampler device developed by Rolls Royce (Courtesy of Rolls-Royce plc [1])

■ Mechanism

Scoop sampling has been around since the late 1980's but has gained wider acceptance in the industry only within the last few years with advances in technology allowing for increased availability, portability, and faster cutting speeds [2]. Sampling is carried out through a wearing process and for this purpose a cup-shaped cutter blade spins around its axis. Not only the cutter blade spins around its axis, it also rotates around the cutter feed arm so as to cut a lens-shaped sample from the work piece. Due to changes in the angle of blade during rotating operation, the torque must be transmitted to the blade via a flexible arm (flexible drive shaft).

For this reason, the design of this section is extremely important. Working mechanism of the cutting blade is shown typically in Fig. 2.

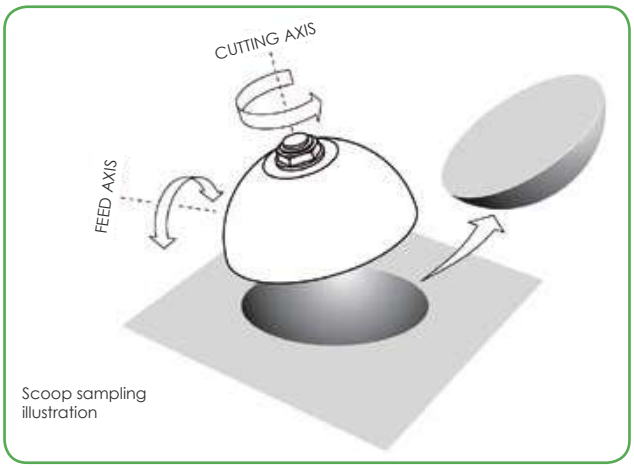

Fig. 2 – Schematic working mechanism of the scoop sampler's cutting blade (Courtesy of Rolls-Royce plc [1])

Wearing process must be carried out so that a constant feed force is applied to the blade during its operation. In various kinds of this device, gears and springs are used to apply the required force to the feed arm.

A vernier equipped with a slider is typically provided allowing for adjusting required specimen thickness.

The device must be able to accommodate surfaces with different angles, so a hinge type connection is typically chosen at the base of the device.

■ Cutting Blade Geometry

Depending on the geometry of the required specimen and operation of the sampling device, the blade is designed to cut specimens of 25.4 mm in diameter and 4 mm deep (with an accuracy of 0.2 mm) out from the surface of a part. The only possibility for doing so is application of a spherical blade that cuts the sample by rotating around its central axis.

Due to geometric limitations and following careful analyses and calculations, the cutting blade of the would-be MAPNA Turbine scoop sampling device is determined to be a hemisphere with a 54 mm diameter, shown in Fig. 3. The edges of the blade is coated with abrasive particles.

Fig. 3 – A photo of the cup-shaped cutting blade of the MAPNA Turbine scoop sampling device

■ Cutting Blade Material

Diamond is the hardest known material, and its average hardness is five times that of cementite carbides. Diamond boasts a very high hardness value, excellent abrasion resistance, good thermal conductivity, high surface smoothness, very high compressive strength, and low thermal expansion which caters for dimensional compatibility in cutting as well as ensured uniform and accurate dimensions in the work piece. Furthermore, due to chemical neutrality of diamond and its low friction coefficient in contact with most materials during cutting, the work piece chip welding to the tool edge phenomenon does not occur. Diamond tools wear quickly when cutting soft and low carbon steels however, and machining of ferrous and cast iron alloys using diamond tools is generally not recommended.

Cubic Boron Nitride (CBN) is the hardest known material after diamond. Its high thermal stability and resistance properties to chemical attack make it suitable for machining of ferrous materials, in areas where diamond abrasive tools are not normally employed. CBN is known for thermal resistance up to a temperature of 1000 °C. CBN is free from carbon and does not react with steel. This property of CBN makes it an ideal choice for grinding of hardened steel [3]. Application of CBN is recommended for chipping tools for hardening carbon and alloy steels, hardened tools, cast irons, especially nickel and cobalt-based super alloys as well as powder metallurgy parts, plastics and graphite. CBN is the best choice, according to the researches carried out on one hand, and the ability to cut a diverse range of metal alloys on the other hand.

The nature of bonding of the coating on the cutter blade is very important. The selection of bonding depends on the functional factors of the tool such as speed, type of cutting operation, required accuracy, and material. For complete abrasion, the abrasive particles of diamond or CBN must be placed close to each other, on the edges of the cutting tool. The adhesive binds the abrasive particles, and during cutting, it must be the abrasive particles to separate from the surface of the cutter edge and sharper particles are replaced to continue the operation. Different types of adhesives are used in manufacturing cutting tools; each of them giving specific properties to the blade. For this reason, application of the following blades was thoroughly investigated and performance tests were carried out.

- Metal bonded diamond grinding wheel
- Metal bonded CBN grinding wheel
- Resin bonded diamond grinding wheel
- Resin bonded CBN grinding wheel
- Polyimide bonded diamond grinding wheel
- Polyimide bonded CBN grinding wheel
- Vitrified bonded diamond grinding wheel
- Vitrified bonded CBN grinding wheel
- Electroplate coating grinding wheel

Following a complete review of the resources and research on blade tools carried out by renowned corporations, application of the electroplated bond was selected. Utilization of the electroplated bonds was agreed upon with a single layer of CBN coating to be deposited uniformly over the steel body of the cutter via electroplating process [3].

Selection of the CBN particles grit size was carried out based on finished surface requirements. The effects of mesh sizes of 90-180 μm on surface roughness of the cutting zone were also thoroughly investigated.

The blade substrate material is usually selected from high-alloy steel or high nickel alloy steel.

This selection is based on the thickness of blade, speed, and feed. Performance of three materials including high nickel steel, tool steel and carbon steel was investigated in the course of this project.

For minimizing the chipping volume from the surface, scoop sampler's blade should be as thin as possible. The blade strength is reduced consequently and hence experimental analyses become necessary to reach an optimum value for the blade thickness.

The results of the experimental investigations carried out using three different thickness values of 0.6, 0.8 and 1 mm are presented in subsequent paragraphs.

In order to determine the scoop sampling device specifications in more detail, a primary setup was designed and developed, as shown in Fig. 4.

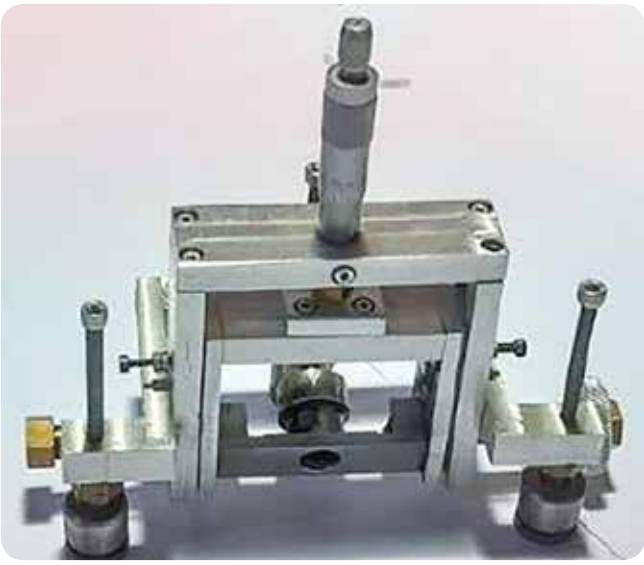

Fig. 4 – Primary setup of the designed and developed scoop sampling device

Experimental Investigations

At this stage and following some careful analyses, research and tests, the design of the device concluded with the following specifications:

- Utilization of a thrust bearing for the secondary rotation mechanism of the tool for increased accuracy and convenient rotation
- Application of a gear box mechanism for the rotary bearing feed mechanism
- Utilization of a self-locking screw mechanism in the gearbox that would prevent any serious damage to the tool and work piece as well as providing for increased controllability of the feed
- Using an adjusting mechanism in the rails for increased accuracy of the tool
- Using a 25000 rpm driving motor for rotating the cutter
- Utilization of a coupling connection 6 mm in diameter for reduced coupling vibrations
- Utilization of a vernier equipped with a slider for specimen thickness adjustment

As discussed previously, three sets of blades with different materials, various specifications and same geometrical dimensions were manufactured. The specifications of these blades are listed in Tables 1 to 3. Each set of cutter blade tools was then installed on the primary setup device and sampling was carried out from the surface of a constant sheet metal under same operating conditions.

Table 1 – Specifications of cutter blade tools made from high-nickel alloy steel

Tool No	Substrate Material	Substrate Thickness	FEPA Standard of CBN	CBN Standard	Mesh Size Min.-Max.
1	High Nickel Alloy Steel	0.6 mm	BN 181	80/100	150 - 180 µm
2	High Nickel Alloy Steel	0.6 mm	BN 151	120/140	125 - 150 µm
3	High Nickel Alloy Steel	0.6 mm	BN 126	140/170	106 - 125 µm
4	High Nickel Alloy Steel	0.6 mm	BN 107	170/200	90 - 106 µm

Table 2 – Specifications of cutter blade tools made from tool steel

Tool No	Substrate Material	Substrate Thickness	FEPA Standard of CBN	CBN Standard	Mesh Size Min.-Max.
5	Tool Steel	1 mm	BN 181	80/100	150 - 180 µm
6	Tool Steel	1 mm	BN 151	120/140	125 - 150 µm

Table 3 – Specifications of cutter blade tools made from carbon steel

Tool No	Substrate Material	Substrate Thickness	EFPA Standard of CBN	CBN Standard	Mesh Size Min.-Max.
7	Carbon Steel	0.8	BN 151	120/140	125 - 150 µm
8	Carbon Steel	0.8	BN 126	140/170	106 - 125 µm
9	Carbon Steel	0.8	BN 107	170/200	90 - 106 µm
10	Carbon Steel	1.0	BN 151	120/140	125 - 150 µm
11	Carbon Steel	1.0	BN 126	140/170	106 - 125 µm
12	Carbon Steel	1.0	BN 107	170/200	90 - 106 µm

The following parameters were inspected and analyzed during and after implementation of each sampling process:

- Control of particle adhesion to the tool's substrate
- Inspection of blade deformation
- Control of blade and work piece temperature during cutting process

According to the inspections and investigations performed, the following conclusions could be drawn:

■ As the particle size decreases, the cutting speed of the device also decreases, on the contrary, the adhesion to the surface improves and the cutting depth increases

Experiments indicate that finer CBN particles on tools No. 3&4 have higher adhesion and were able to complete up to around 50% of the desired cutting process while tools No. 1&2 did not seem to have sufficient adhesion to the surface of the work piece and after a short period of machining, a high percentage of particles were separated from the surface of the cutting tool. The latter tools both ceased to operate after a 30% advance due to significant reduction in the number of remained abrasive particles.

Tool No. 6 with finer abrasive particles showed higher adhesion to the surface than tool No. 5. Generally, the adhesion and wear resistance of tool No. 6 was better than tool No. 5. For tools No. 7, 8, and 9, due to low adhesion to the surface, more CBN particles were separated during cutting and the cutting process was not completed in these cases.

■ It is necessary to have at least 1 mm-thick material to prevent tool deformation

Deformation was observed in all tool specimens with material thickness of below 1 mm.

■ To prevent overheating of the work piece, high thermal conductivity material must be used for blade tool

During the cutting process, temperatures of the work piece and cutting blades were measured using an infrared screening camera. Recorded temperature measurements for two blade tool specimens are presented in Fig. 5.

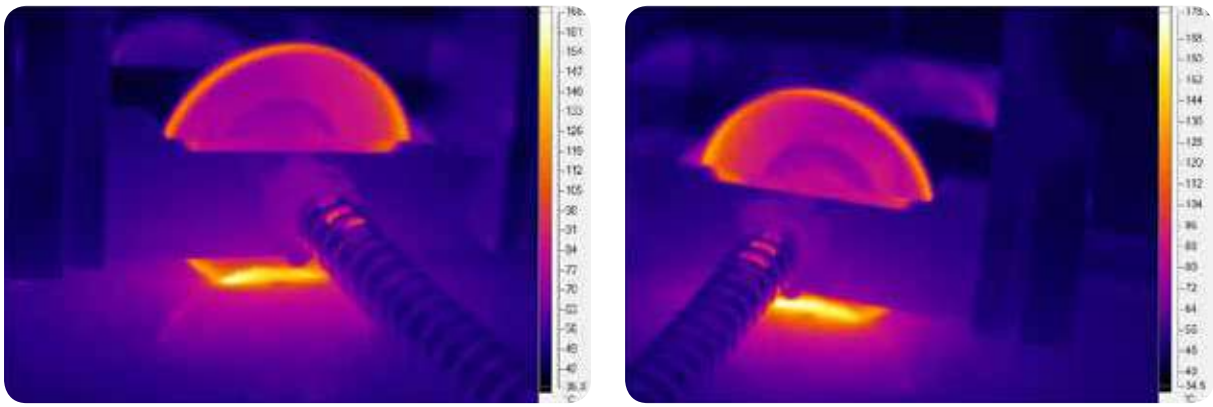

Fig. 5 – Temperature distribution over the blade and work piece for blade tool No. 10 (left) and blade tool No. 11 (right)

High nickel alloy steel and carbon steel had the lowest and highest thermal conductivity, respectively. Moreover, as the CBN particle sizes decreased, the temperatures increased during the cutting process.

A typical scooped sample besides its corresponding sampling zone dug on the surface of the work piece used for the mentioned experimental investigations is shown in Fig. 6.

Fig. 6 – Typical scooped sample taken besides the sampling zone dug on the surface of a work piece (top), specimen size measurements (bottom)

Subsequent to in-depth experimental investigations carried out, the final specifications of the cutting blade tool were found to be as follows:

Material: Carbon steel

Thickness: 1 mm

Mesh Configuration: BN126

A photo of the final MAPNA Turbine's scoop sampling device while cutting a sample from the surface of a workpiece is shown in Fig. 7.

Fig. 7 – Final setup of MAPNA Turbine's scoop sampling device in action

Concluding Remarks

A complete scoop sampling device was designed and developed to allow for detailed investigation of the mechanical properties, micro-structural analyses and residual life assessment of aged materials in different critical parts and components of power plant equipment. A sampling scheme was designed and developed for scooping out 25.4 mm lens-shaped samples. Specifications of different parts, elements and components of the device in general and its cutter blade in particular were carefully investigated, experimented and concluded. According to the investigations carried out, a cup-shaped cutter blade with a diameter of 54 mm, made from 1 mm-thick carbon steel was suitable for substrate of the blade. The edges of the blade were coated with single layer CBN particles of 126BN mesh using electroplating process.

References

[1] Rolls-Royce, "Capability Sheet: Scoop Sampling", www.rolls-royce.com, 2010

[2] Douglas Marriott, Shannon Read, Arun Sreeranganathan, "The use of miniature test specimen in fitness-for service evaluation", *Inspectioneering Journal,* May/June, 2016, PP.1-3

[3] Kundan Kumar1, K. Madhusoodanan, R. N.Singh, J.K. Chakravartty, B.K.Dutta and R. K. Sinha, "Development and Validation of In-Situ Boat Sampling Technique for Mechanical Property Evaluation and Life Management of TAPS Core Shroud", *International Journal of Engineering Research & Technology (IJERT),* July – 2014, PP. 1702-1708.

5

Moving Into the Industry 4.0 Future; MAPNA MIND at the Helm

Shakibafar, Mohsen
Taheri, Mahsa

MAPNA Electric & Control, Engineering & Manufacturing Co. (MECO)

Introduction

Fourth industrial revolution, Industry 4.0 (4IR) refers to a new phase in the industrial revolution. It was originated by the German government at the Davos conference in 2011. Examples of developments that have begun in this period are smart cities, 3D printers, etc. The basis for this development is the connection of experts, data, and sensors to one another. In this revolution, industries are using tools such as IIoT[1], cloud computing, artificial intelligence, and CPS[2]. CPS means creation of a digital version of the industry in the cloud. This digital version is known as the Digital Twin. This digital version brings about decentralization of data, experience, analysis, monitoring, and management in the industry.

The Fourth Industrial Revolution, just like other industrial revolutions, has the potential to increase industry incomes and improve the quality of life. According to a recent analysis [1], by 2022, industries moving in the direction of Industry 4.0 will have a 10% increase in profits, and by 2024, its trade value will reach $155 billion. In addition, the arrival of the 4IR is expected to create up to $3.7 trillion in value to global manufacturing [2].

Some of the most important factors that indicate why we should move towards the 4IR are as follows:

- Customer requirements
- Destruction of industrial data
- Easy access to data and analysis
- Solving more problems more quickly
- Equipment support
- Creating comparison facilities
- Ability to use artificial intelligence
- Increased creativity

According to the 4IR principles, the following are expected:

- Interconnection
- Information transparency
- Technical assistance
- Decentralized decision making

So, a comprehensive platform is required for achieving these goals, in which after connecting the data, various tools can be created to help industry owners.

[1] Industrial Internet of Things

[2] Cyber Physical System

MAPNA MIND

To move towards the 4IR, a Platform is required that can collect industrial data with thorough security, store it in appropriate data models and keep it readily available. Such a platform should be able to operate in the form of IoT and IIoT and have a programmable PaaS[3] layer and a web-based SaaS[4] layer that has the necessary facilities for programming industrial data, analysis, monitoring, and benchmarking of industrial data. In this regard, due to the enormous amount of information and processing, a very powerful IaaS[5] service is required.

To serve this purpose, a platform called MAPNA MIND was developed within MAPNA Group to create powerful monitoring and analysis tools and to make the development of industrial applications possible.

MAPNA MIND Architecture

As mentioned earlier, the architecture of this platform must be cloud-based. Fig. 1 shows a simplified representation of such architecture.

Fig. 1 – MAPNA MIND cloud-based architecture

As shown in Fig. 1, using the MAPNA MIND the product is developed within the two main layers of the cloud.

The MIND Cloud covers the PaaS layer, where users can program industrial data offline and even online, and to develop required applications accordingly.

MIND Studio also has many features by which users can perform all kinds of monitoring and analysis.

As a result, MAPNA MIND includes the following main products:

- MIND Studio (Web/Android)
- MIND Cloud
- MIND App
- MIND Edge

The MIND app is also developed by MIND Cloud, and users can use this feature.

MAPNA MIND is capable of receiving data from industries to analyze and display everywhere.

A simplified representation of the main components of MAPNA MIND is shown in Fig. 2.

[3] Platform as a service
[4] Software as a service
[5] Infrastructure as a service

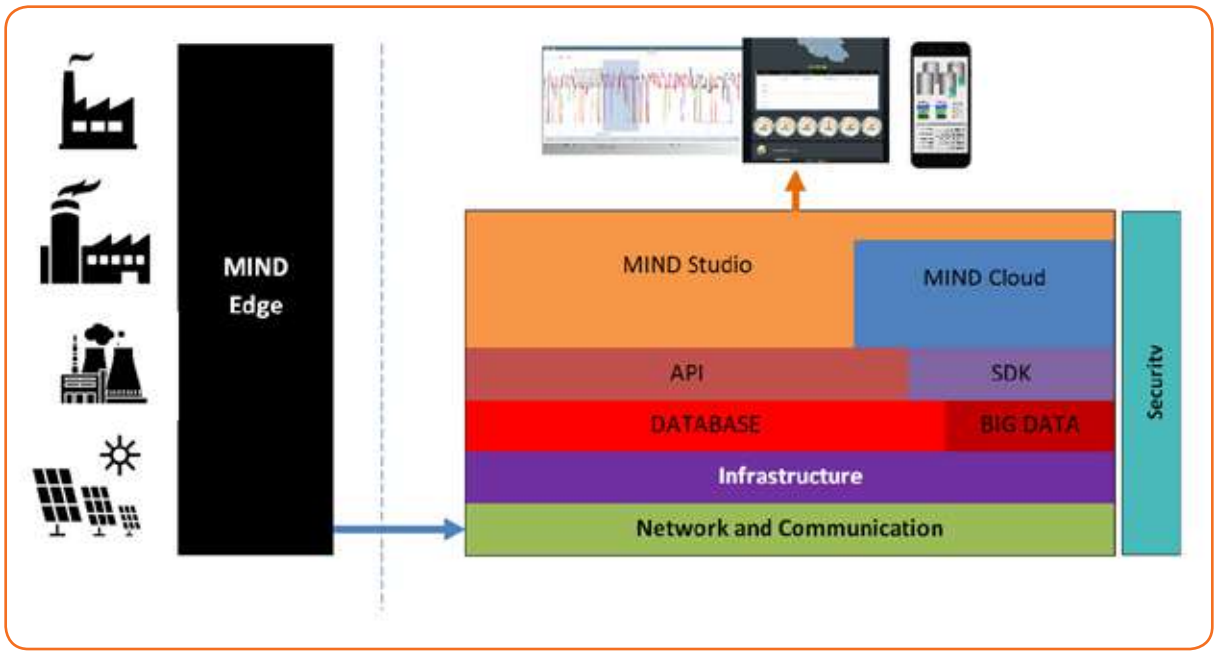

Fig. 2 – Simplified representation of MAPNA MIND architecture & components

As shown in Fig. 2, the MAPNA MIND platform contains important components that perform various tasks. The functions of layers such as Network or Database were specified. In the following, the index sections of the platform are introduced and elaborated on.

■ Mind Edge

MAPNA MIND platform can be connected to in various industries, which is most related to the MIND Edge. This software must be connected to industries that support one of these protocols: OPC UA, OPC DA, MQTT, Modbus TCP, ActiveMQ

In MIND Edge, the data is stored for more than ten days, so that if the connection to the data center is lost, the data will be sent again. The MIND Edge system can send data to the center every second and keep it up to date.

MIND Edge is the most secure layer of the MAPNA MIND since it is electronically separated from the industrial networks of the power plant, which rules out any penetration into the industrial network if there is any such incident within the MAPNA MIND network.

Fig. 3 shows the inner layers of MIND Edge.

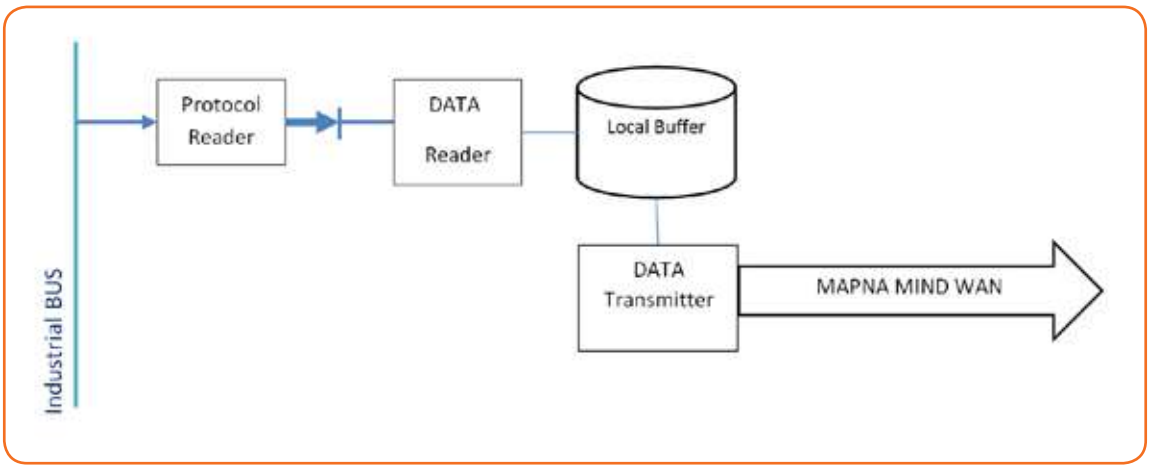

Fig. 3 – MIND Edge layers

■ Network Layer

As shown in the Fig. 2, the lowest layer of MAPNA MIND is the Network section which includes the connection of industries, switches, and routers. In other words, this layer is supposed to transfer data from industries to the data sector and store information in the data section. MAPNA MIND network operates unilaterally in this area and does not send any commands to the industry. In this section, all security principles have been observed, including the following:

- Utilization of security tools such as Next-Generation Firewall
- Data Encryption
- VPN and Tunneling

■ Data Layer

One of the main challenges that industries have long faced is the data management . Because most industries are not able to keep their data for a long time and after a period ranging from 3 months to 5 years, the data is usually overwritten or lost.

The data layer is tasked with keeping the data[6] of connected industries in the cloud within the scope specified in the contract. This will allow industry professionals and managers to access long-term data history to be used in applications and monitoring tools.

Data is completely secure in MAPNA MIND platform because no user, not even the developers, has direct access to this layer.

Data is compressed after a certain period. Therefore, the data layer can provide users with practically unlimited space for information.

■ API Layer

As mentioned earlier, no one is able to connect directly to the data and the connection is only possible via the API layer. This layer provides all the necessary tools for the higher layers with complete security. For example, no external user can access the database and send a query on it and must use GetDataSignal APIs. This protects the database from inadvertent or malicious changes.

This layer includes various services for reporting, chart designing, and monitoring. All of these services are connected to higher layers through an important service called Gateway.

■ SDK Layer

This layer can be used by MAPNA MIND developers. A complete guide to this part will follow. The SDK (Software Development Kit) comprises library functions that allow programmers to access industry data.

■ MIND Cloud

As mentioned earlier, this section plays the role of the PaaS layer within MAPNA MIND. Therefore users have the opportunity to develop the required applications on their own and put them on the cloud. Fig. 4 represents the programming languages supported by MIND Cloud.

[6] Data important to the industry owner and meant to be transferred to the MAPNA MIND

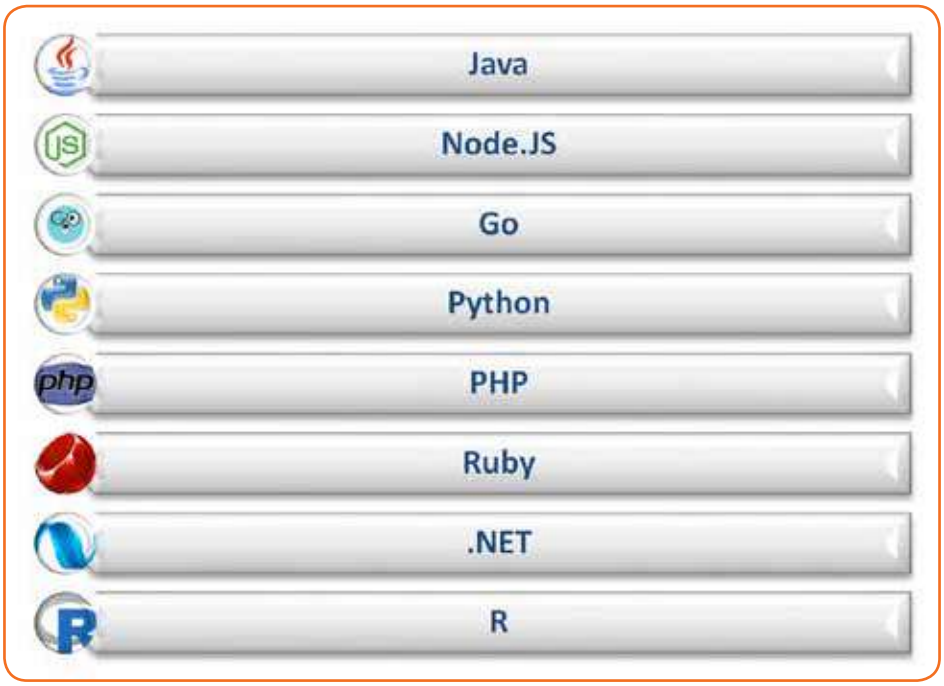

Fig. 4 – MIND Cloud supported programming languages

All software developed using any of these programming languages are able to be deployed in the MAPNA MIND Cloud.

Within the MIND Cloud, library functions are created to read online/offline industrial data and create an alarm if necessary. For example, a user can develop a program to perform some calculations on a power plant data and when a problem occurs, this program will create an alarm to show on the Alarm/Event page in the Mind Studio.

■ MIND Studio

As shown in Fig. 2, MIND Studio is the outer layer of the platform (SaaS layer in the cloud) through which users will be able to communicate with the platform and utilize its features. MIND Studio is developed in web and Android so it can be used with all operating systems and computers. MIND Studio features are outlined below:

► Dashboard Management

Via this section, a user can view and manage all the elements under their supervision in general.

Fig. 5 – A snapshot of MIND Studio dashboard management tool

► Chart Management

Charts are among the most important tools for analyzing and monitoring purposes. Through different chart types of online and/or offline data, aggregated or raw data from several years are available to experts and managers within the Mind Studio, as shown in Fig. 6.

Fig. 6 – A snapshot of available chart data within the MIND Studio

► Online Monitoring

One of the features of MIND Studio is the ability to monitor the entire fleet simultaneously. Users can design and store their monitoring layer and HMI in this platform and provide it to other users so that they can monitor their fleet remotely.

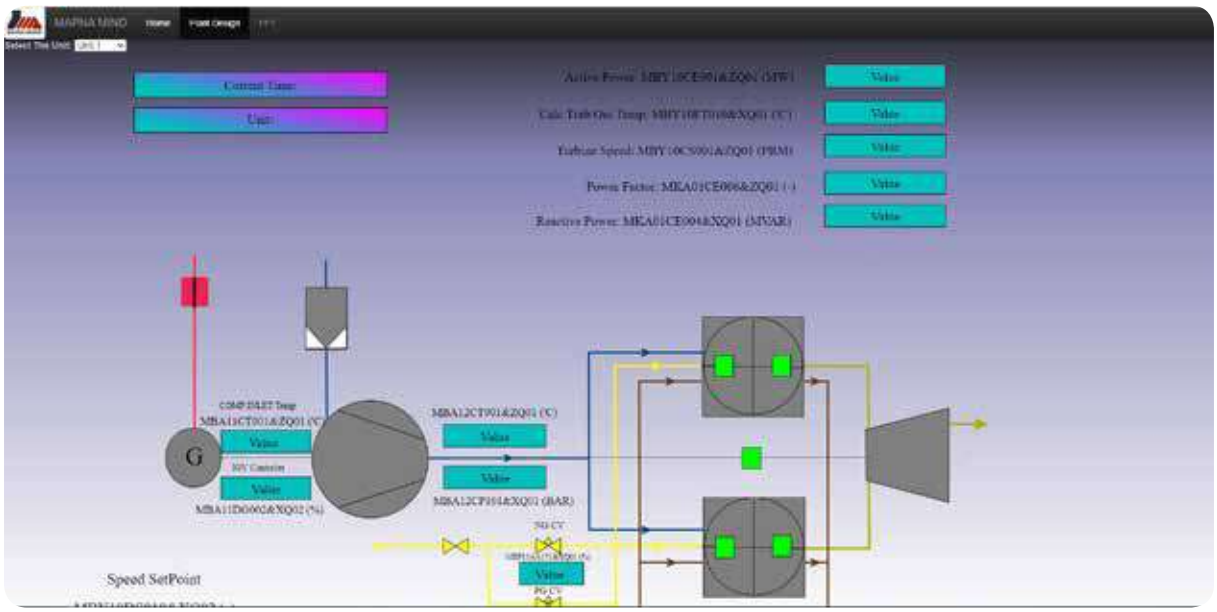

Fig. 7 – A snapshot of online monitoring feature available within the MIND Studio

► **Alarm Management**

Alarm/Event section is deemed one of the most important monitoring tools in any industrial application, because it is not possible for users to constantly analyze all the data, it is of vital importance for a monitoring system to come to a conclusion and issue a warning if necessary following the implementation of some simple or complex analyses. Issuance, control and management of such warnings are carried out within the alarm management section of the MIND Studio.

► **Report Management**

One of the most powerful tools of MIND Studio is its Report section, which can provide the users with the following benefits:

- Ability to generate different report formats such as MS Word, Pdf, … utilizing tables, charts, etc.
- Ability to generate scheduled reports, i.e., daily, weekly or monthly
- Ability to generate instant on-demand reports
- Ability to send out reports in MAPNA MIND network

► **Offline /Online Data Display**

Access to offline data in the form of tables is possible in the Historian tool. This tool enables the user to access all the data gathered since connection was established to the MAPNA MIND. Via this section, the user can access to the raw or aggregated data. Online data could also be accessed using any of the following features: Watch Tool, Dashboard, Online Chart, HMI.

Watch tool enables the user to monitor and compare different signals from the entire fleet.

► **User & Ticket Management**

User management and access level stipulation of different users are of prime importance when it comes to operating system security. To improve the security and to protect each client's data, user management is provided within the MIND Studio.

Ticket management is also one of the most important features of the MAPNA MIND platform by enabling communication and referral of tasks and questions to designated experts which is achieved via MAPNA MIND Studio. When a ticket is sent to the expert, a notification is sent to them, which must be answered or referred to other experts within a certain time period. It allows for sending images of breakdowns, sounds of mechanical anomalies or alarm sounds.

Signal selector, reviewing specific system information such as temperatures, pressures and vibrations are some other features provided by MAPNA MIND Studio. Different applications could also be developed and integrated into the MAPNA MIND platform. Once installed through MIND App, these applications will become visible and accessible via the Application menu.

References

[1] A. Doust, "Will Industry 4.0 See Sustainable Growth, Or Will The Bubble Burst?"

Forbes, October 3rd, 2019 (Online). Available at:

http://www.forbes.com/sites/forbestechcouncil/2019/10/03/will-industry-4-0-see-sustainable-growth-or-will-the-bubble-burst/

[2] H. Leurent, E. De Boer and D. H. Diaz, "The Fourth Industrial Revolution and the factories of the future" *World Economic Forum,* August 10th, 2018 (Online). Available at:

https://www.weforum.org/agenda/2018/08/3-lessons-from-the-lighthouses-beaming-the-way-for-the-4ir/


Management
Building

Head Office:
231 Mirdamad Ave. Tehran, I.R.Iran.
P.O.Box: 15875-5643
Tel: +98 (21) 22908581
Fax: +98 (21) 22908654

Factory:
Mapna blvd., Fardis, Karaj, I.R.Iran.
Post code: 31676-43594
Tel: +98 (26) 36630010
Fax: +98 (26) 36612734

www.mapnaturbine.com
tr@mapnaturbine.com

© MAPNA Group 2021

The technical and other data contained in this Technical Review is provided for information only and may not apply in all cases.

GR488-0